Article

V Magic Angle Spinning NMR Spectroscopy of Six-Coordinate Lindqvist Oxoanions: A Sensitive Probe for the Electronic Environment in Vanadium-Containing Polyoxometalates. Counterions Dictate the V Fine Structure Constants in Polyoxometalate Solids

Wenlin Huang, Louis Todaro, Lynn C. Francesconi, and Tatyana Polenova

J. Am. Chem. Soc., **2003**, 125 (19), 5928-5938• DOI: 10.1021/ja029246p • Publication Date (Web): 17 April 2003

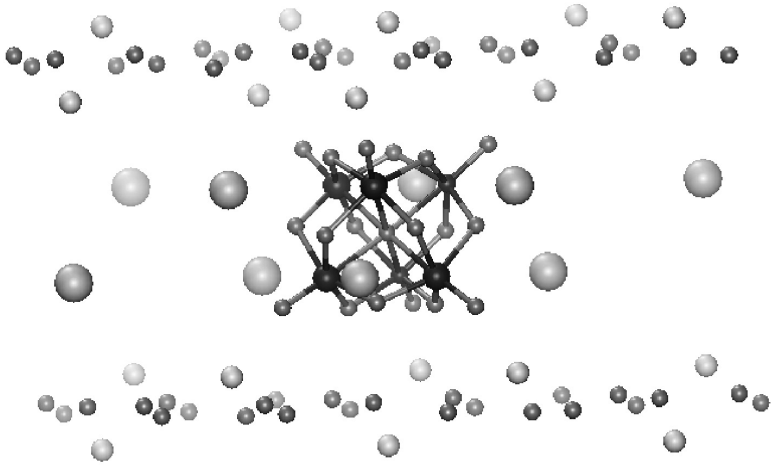

J|A|C|S
ARTICLES
Published on Web 04/17/2003

^{51}V Magic Angle Spinning NMR Spectroscopy of Six-Coordinate Lindqvist Oxoanions: A Sensitive Probe for the Electronic Environment in Vanadium-Containing Polyoxometalates. Counterions Dictate the ^{51}V Fine Structure Constants in Polyoxometalate Solids

Wenlin Huang, Louis Todaro, Lynn C. Francesconi, and Tatyana Polenova*

Contribution from the Department of Chemistry, City University of New York—Hunter College and The Graduate Center, 695 Park Avenue, New York, New York 10021

Received November 6, 2002; E-mail: tpolenov@hunter.cuny.edu

Abstract: Geometric and electronic environments of vanadium have been addressed by ^{51}V magic angle spinning NMR spectroscopy of six-coordinated polyoxometalate solids. $(C_4H_9)_4N^+$ and mixed Na^+/Cs^+ salts of the Lindqvist-type mono- and divanadium-substituted oxotungstates, $[VW_5O_{19}]^{3-}$ and $[V_2W_4O_{19}]^{4-}$, have been prepared as microcrystalline and crystalline solids. The solid-state NMR spectra reflect the details of the local environment of the vanadium site in these hexametalate solids via the anisotropic quadrupolar and chemical shielding interactions. Remarkably, these ^{51}V fine structure constants in the solid state are dictated by the nature and geometry of the countercations. Electrostatic calculations of the electric field gradients at the vanadium atoms have been performed. Experimental trends are well reproduced with the simple electrostatic model, and explain the sensitivity of the anisotropic NMR parameters to the changes in the cationic environment at the vanadium site.

Introduction

Polyoxometalates (POMs) are attractive for the design of new materials, due to diverse chemistry and favorable structural and electronic properties.[1−3] Vanadium-containing polyoxometalates have become the object of interest in optoelectronics due to their putative electro-, photo-, and thermochromism, and potential applications as solid nanocomposite molecular devices.[3−6] Mixed- valence V(IV)−V(V) clusters possess unusual magnetic properties.[7]

The design of polyoxometalate materials with targeted three-dimensional structures has recently emerged as an active research area.[4,8,9] Despite a number of successful efforts, much experimental and theoretical work remains before this can become a general approach. For technological applications, the following factors are of paramount importance: (i) the synthetic procedure has to be consistent as small variations in conditions (pH, solvents, etc.) can yield impurities or undesirable products; (ii) counterions have an immediate effect both on the structure[10] and on the physicochemical properties of POM solids;[11] (iii) the morphology of solid materials has to be controlled as an altered degree of bulk order may be detrimental to the properties.

A number of techniques have been traditionally used for characterization of various aspects of solid POMs,[3] and their arsenal is constantly expanding due to the growing need for advanced molecular probes. Among the spectroscopic techniques, solid-state NMR spectroscopy has been an important analytical tool for studies of inorganic materials and biological solids. Solid-state NMR experiments can yield quantitative site-specific information for amorphous and crystalline solids, in the bulk, on surfaces, and at the interfaces.[12] Multinuclear solid-state NMR has been applied to probe various aspects of the structure and reactivity of heteropoly systems,[13−19] but the potential of solids NMR for the analysis of POMs has not been fully realized. In particular, ^{51}V solid-state NMR spectroscopy is rapidly emerging as a technique for the analysis of vanadium-containing systems. Solid-state ^{51}V NMR has been applied to

(1) Pope, M. T.; Müller, A. *Angew. Chem., Int. Ed. Engl.* **1991**, *30*, 34−48.
(2) Coronado, E.; Gómez-García, C. J. *Chem. Rev.* **1998**, *98*, 273−296.
(3) Katsoulis, D. E. *Chem. Rev.* **1998**, *98*, 359−387.
(4) Gomez-Romero, P. *Adv. Mater.* **2001**, *13*, 163−174.
(5) Yamase, T. *Chem. Rev.* **1998**, *98*, 307−325.
(6) Liu, S. Q.; Kurth, D. G.; Mohwald, H.; Volkmer, D. *Adv. Mater.* **2002**, *14*, 225−229.
(7) Müller, A.; Peters, F.; Pope, M. T.; Gatteschi, D. *Chem. Rev.* **1998**, *98*, 239−271.
(8) Johnson, B. J. S.; Schroden, R. C.; Zhu, C.; Stein, A. *Inorg. Chem.* **2001**, *40*, 5972−5978.
(9) Johnson, B. J. S.; Schroden, R. C.; Zhu, C.; Young, V. G.; Stein, A. *Inorg. Chem.* **2002**, *41*, 2213−2218.
(10) Kim, K.-C.; Pope, M. T. *J. Am. Chem. Soc.* **1999**, *121*, 8512−8517.
(11) Grigoriev, V. A.; Hill, G. L.; Weinstock, I. A. *J. Am. Chem. Soc.* **2000**, *122*, 3544−3545.
(12) Eckert, H. *Curr. Opin. Solid State Mater.* **1996**, *1*, 465−476.
(13) Blouet-Crusson, E.; Rigole, M.; Fournier, M.; Aboukais, A.; Daubrege, F.; Hecquet, G.; Guelton, M. *Appl. Catal. A* **1999**, *178*, 69−83.
(14) Nakata, S.; Tanaka, Y.; Asaoka, S.; Nakamura, M. *J. Mol. Struct.* **1998**, *441*, 267−281.
(15) Kozhevnikov, I. V.; Sinnema, A.; vanBekkum, H.; Fournier, M. *Catal. Lett.* **1996**, *41*, 153−157.
(16) Kozhevnikov, I. V. *Chem. Rev.* **1998**, *98*, 171−198.
(17) Torok, B.; Palinko, I.; Molnar, A.; Rozsa-Tarjani, M. *J. Mol. Struct.* **1999**, *483*, 329−332.
(18) Baba, T.; Ono, Y. *Annu. Rep. NMR Spectrosc.* **1999**, *38*, 355−390.
(19) Damyanova, S.; Fierro, J. L. G.; Sobrados, I.; Sanz, J. *Langmuir* **1999**, *15*, 469−476.

10.1021/ja029246p CCC: $25.00

address a number of systems, including inorganic vanadates,[20−26] vanadium-based catalysts,[27−30] oxovanadium(V) alkoxides,[31] zeolites,[32] and metallorganic complexes.[33,34]

In this paper, we demonstrate that ^{51}V solid-state magic angle spinning NMR spectroscopy is a very sensitive probe of the local geometric and electronic environment of the vanadium site in six-coordinate Lindqvist-type vanadium-substituted oxotungstates. We discuss the spectroscopic properties of a series of four molecules, $(C_4H_9)_4N^+$ and mixed Na^+/Cs^+ salts of $[VW_5O_{19}]^{3-}$ and $[V_2W_4O_{19}]^{4-}$, whereas each compound has been prepared as a powder and diffraction-quality crystals. We address the effect of the cation and the number of vanadium atoms in the oxotungstate core on the solid-state NMR spectra. The solid-state NMR measurements presented herein reveal for the first time that ^{51}V fine structure constants of hexametalates in the solid state, namely, the quadrupolar and chemical shielding anisotropies, are dictated by the nature and geometry of the countercations. ^{51}V solid-state NMR spectroscopy can thus become a valuable analytical tool for probing the local electronic environment in polyoxometalate materials.

Theoretical Considerations for ^{51}V Solid-State NMR Spectroscopy. Quadrupolar and Chemical Shielding Anisotropies

^{51}V is a half-integer quadrupolar nucleus ($I = 7/2$) with high natural abundance (99.8%) and relatively high gyromagnetic ratio (Larmor frequency of 105.2 MHz at 9.4 T). The small quadrupolar moment allows direct observation of vanadium, and due to the favorable magnetic properties, small quantities of vanadium can be readily detected.

For half-integer spin nuclei, such as ^{51}V, the solid-state NMR spectra are dominated by a combination of the quadrupolar interaction (the interaction between the electric quadrupole moment of the nucleus and the electric field gradient on the nuclear site) and nuclear magnetic shielding anisotropy. The latter is observable in the NMR spectra via the symmetric part of the chemical shielding anisotropy (CSA) tensor (see refs 25 and 35[25,35] and references therein). The different magnitudes and different symmetry properties of the quadrupolar and chemical shielding anisotropies allow these tensorial quantities to be extracted from a single spectrum, along with the mutual orientations of the quadrupolar and CSA tensors.[25] The total Hamiltonian in addition includes the dipolar and the radio-frequency terms and can be expressed as

$$\mathscr{H} = \mathscr{H}_{\text{Zeeman}} + \mathscr{H}_{\text{RF}} + \mathscr{H}_{\text{DIP}} + \mathscr{H}_{\text{Q}} + \mathscr{H}_{\text{CSA}} \quad (1)$$

The first three terms represent the Zeeman, the radiofrequency field, and the dipolar interactions. The last two terms are the quadrupolar and CSA interactions, which dictate the spectral shape. They are conveniently expressed in a spherical tensor notation in terms of the spatial (R_{mn}) and spin (T_{mn}) variables:[36]

$$\mathscr{H}_{\text{Q}}^{(1)} = \frac{eQ}{4S(2S-1)} R_{20}^{\text{Q}} T_{20}^{\text{S}} = \omega_{\text{Q}}[3S_z^2 - S(S+1)] \quad (2)$$

$$\mathscr{H}_{\text{Q}}^{(2)} = \frac{C_{\text{Q}}}{\omega_0} \sum_{m \neq 0} \frac{R_{2m} R_{2-m} [T_{2m}, T_{2-m}]}{2m} \quad (3)$$

$$\mathscr{H}_{\text{CSA}} = -\gamma(R_{00}^{\text{CS}} T_{00}^{\text{S}} + R_{20}^{\text{CS}} T_{20}^{\text{S}}) = (\omega_{\text{CS}}^{\text{iso}} + \omega_{\text{CS}}^{\text{aniso}}) S_z \quad (4)$$

$\mathscr{H}_{\text{Q}}^{(1)}$ and $\mathscr{H}_{\text{Q}}^{(2)}$ are the first- and second-order quadrupolar interactions. The quadrupolar and CSA tensor elements are defined in a spherical harmonics basis set according to the standard notation[37,38]

$$C_{\text{Q}} = \frac{eQV_{zz}}{h} \qquad \eta_{\text{Q}} = \frac{V_{yy} - V_{xx}}{V_{zz}}$$

$$\delta_\sigma = \delta_{zz} - \delta_{iso} \qquad \eta_\sigma = \frac{\delta_{yy} - \delta_{xx}}{\delta_{zz} - \delta_{\text{iso}}}$$

$$\delta_{\text{iso}} = {}^1/_3(\delta_{xx} + \delta_{yy} + \delta_{zz}) \quad (5)$$

where C_{Q} is the quadrupolar coupling constant (MHz) and V_{xx}, V_{yy}, and V_{zz} are the principal components of the electric field gradient (EFG) tensor, with $V_{zz} = eq$ being its largest principal component, and $|V_{zz}| \geq |V_{yy}| \geq |V_{xx}|$. C_{Q} defines the overall breadth of the spectral envelope. Q is the vanadium quadrupole moment (-0.052×10^{-28} V/m^2),[35] e is the electronic charge, and h is the Planck constant. δ_{iso} is the isotropic chemical shift, and δ_{xx}, δ_{yy}, and δ_{zz} are the principal components of the CSA tensor. δ_σ is the anisotropy of the CSA tensor, determining the breadth of the tensor. η_{Q} and η_σ are the asymmetry parameters of the EFG and CSA tensors, defining their skew.

Upon spinning the solid powder sample at the magic angle (54.7°), the second-rank spatial components R_{20} of the tensorial anisotropies of $\mathscr{H}_{\text{Q}}^{(1)}$ and $\mathscr{H}_{\text{CSA}}$ are efficiently averaged into a spinning sideband pattern while the fourth-rank terms of $\mathscr{H}_{\text{Q}}^{(2)}$ are preserved, resulting in a characteristic second-order lineshape.

In Figure 1 of the Supporting Information, a series of ^{51}V hypothetical solid-state static and MAS NMR spectra are shown to illustrate the relationships between the parameters describing the quadrupolar and CSA tensors, and the spectral features.

It has been demonstrated by Skibsted, Nielsen, Jacobsen, and their colleagues in a number of reports that the quadrupolar and

(20) Gubanov, V. A.; Pletnev, R. N.; Lisson, V. N.; Chirkov, A. K. *Spectrosc. Lett.* **1977**, *10*, 527−532.
(21) Hayashi, S.; Hayamizu, K. *Bull. Chem. Soc. Jpn.* **1990**, *63*, 961−963.
(22) Nielsen, U. G.; Jacobsen, H. J.; Skibsted, J. *Inorg. Chem.* **2000**, *39*, 2135−2145.
(23) Nielsen, U. G.; Jacobsen, H. J.; Skibsted, J. *J. Chem. Phys. B* **2001**, *105*, 420−429.
(24) Skibsted, J.; Jacobsen, C. J. H.; Jacobsen, H. J. *Inorg. Chem.* **1998**, *37*, 3083−3092.
(25) Skibsted, J.; Nielsen, N. C.; Bildsøe, H.; Jakobsen, H. J. *Chem. Phys. Lett.* **1992**, *188*, 405−412.
(26) Ganapathy, S.; Schramm, S.; Oldfield, E. *J. Chem. Phys.* **1982**, *77*, 4360−4365.
(27) Eckert, H.; Wachs, I. E. *J. Phys. Chem.* **1989**, *93*, 6796−6805.
(28) Miller, J. M.; Lakshmi, L. J. *J. Mol. Catal., A* **1999**, *144*, 451−459.
(29) Shubin, A. A.; Lapina, O. B.; Bondareva, V. M. *Chem. Phys. Lett.* **1999**, *302*, 341−346.
(30) Lapina, O. B.; Mastikhin, V. M.; Shubin, A. A.; Krasilnikov, V. N.; Zamaraev, K. I. *Prog. NMR Spectrosc.* **1992**, *24*, 457−525.
(31) Crans, D. C.; Felty, R. A.; Chen, H.; Eckert, H.; Das, N. *Inorg. Chem.* **1994**, *33*, 2427−2438.
(32) Park, D. H.; Cheng, C. F.; Klinowski, J. *Bull. Korean Chem. Soc.* **1997**, *18*, 70−75.
(33) Rehder, D.; Paulsen, K.; Basler, W. *J. Magn. Reson.* **1983**, *53*, 500−502.
(34) Hampton, P. D.; Daitch, C. E.; Alam, T. M.; Pruss, E. A. *Inorg. Chem.* **1997**, *36*, 2879−2883.
(35) Smith, M. E.; van Eck, E. R. H. *Prog. NMR Spectrosc.* **1999**, *34*, 159−201.
(36) Frydman, L. *Annu. Rev. Phys. Chem.* **2001**, *52*, 463−498.
(37) Cohen, M. H.; Reif, F. *Solid State Phys.* **1957**, *5*, 321−438.
(38) Schmidt-Rohr, K.; Spiess, H. W. *Multidimensional Solid-State NMR and Polymers*; Hartcourt Brace & Co.: London, San Diego, New York, Boston, Sydney, Tokyo, 1999.

chemical shielding tensors, as well as their relative orientations, can be extracted with high precision by detecting the complete manifold of spinning sidebands from the central and the satellite transitions and subsequently simulating the spectra.[22−25,39−41] These tensorial interactions can be further correlated with the structure and electronic properties at the vanadium site. Approximate estimates of the coordination geometries could be obtained from the quadrupolar coupling constant and the asymmetry parameter of the EFG tensor, using a simple electrostatic model.[42] According to the electrostatic model, the atoms in the first coordination sphere are treated as point charges, whose individual contributions to the electric field gradient on the central atom are combined to yield the net EFG tensor. This model is an oversimplification and cannot be relied on for precise quadrupolar interaction parameters, but it has been quite successful in predicting trends in homologous series of compounds, especially those containing bonds with significant ionic character.[22,23,42] In recent years, the more rigorous quantum mechanical methods have been increasingly applied for calculations of the EFG tensors, which were experimentally found by solid-state NMR, Mössbauer spectroscopy, and other techniques.[43−49]

Experimental Section

Materials. All chemicals were obtained from Aldrich and used without further purification: sodium tungstate dihydrate ($Na_2WO_4 \cdot 2H_2O$), sodium metavanadate ($NaVO_3$), sulfuric acid, tetrabutylammonium bromide [(n-$C_4H_9)_4NBr$], cesium chloride, and hydrochloric acid.

[(n-$C_4H_9)_4N]_3[VW_5O_{19}]$ (**I**), $Cs_3[VW_5O_{19}]$ (**II**), [(n-$C_4H_9)_4N]_3H[V_2W_4O_{19}]$ (**III**), and $Na_2Cs_2[V_2W_4O_{19}]\cdot 6H_2O$ (**IV**) have been synthesized according to literature protocols.[50] Either (n-$C_4H_9)_4NBr$ or CsCl was used at the last step of the synthesis to obtain the corresponding salts of the mono- or divanadium oxoanions. Each of the four compounds has been prepared as a powder or diffraction-quality crystals, except for **II**, which resisted our attempts for crystallization, and therefore, only a powdered sample was studied. The powder samples of **I**−**IV** were prepared by fast precipitation from the concentrated anion solutions using the excess of the corresponding countercation. The crystallization of the individual compounds **I**, **III**, and **IV** is described below.

Crystallization of I and III. Diffraction-quality crystals of [(n-$C_4H_9)_4N]_3[VW_5O_{19}]$ and [(n-$C_4H_9)_4N]_3H[V_2W_4O_{19}]$ were obtained from hot *N*,*N*-dimethylformamide.

Crystallization of IV. Diffraction-quality crystals were obtained by placing the filtrate solution at 4 °C overnight.

X-ray Powder Diffraction. Calcined samples of **I**−**IV** were characterized by X-ray powder diffraction using a Phillips X'Pert MPP instrument with a Cu Kα source with a gas-filled proportional detector. Scans were collected between $2\theta = 0.5°$ and $2\theta = 50.0°$ in increments of 0.01° and counts measured for 2 s at each increment. The measurements were performed at the University of Delaware (Newark, DE).

Single-Crystal X-ray Diffraction. The intensity data for **I**, **III**, and **IV** were measured on an Enraf-Nonius CAD4 diffractometer (graphite-monochromated Cu Kα radiation, $\omega-2\theta$ scans). All data sets were corrected for absorption. Details of the data collection for individual compounds are presented below.

[(n-$C_4H_9)_4N]_3[VW_5O_{19}]$ (I). Of the 10328 independent reflections for $\theta < 60^o$, 7289 were considered observed [$I > 3.0\sigma(I)$]. The structures were solved by a multiple-solution procedure and were refined by full-matrix least squares. In the final refinement, the non-hydrogen atoms were refined anisotropically. The hydrogen atoms were included in the structure factor calculations, but their parameters were not refined. The final discrepancy indices for the 7289 observed reflections were $R = 0.078$ and $R_w = 0.094$. The final difference map peaks (<1.57 e Å^{-3}) were near those of the tungsten and vanadium atoms.

[(n-$C_4H_9)_4N]_3H[V_2W_4O_{19}]$ (III). Of the 10364 independent reflections for $\theta < 60^o$, 6356 were considered observed [$I > 3.0\sigma(I)$]. The structures were solved by a multiple-solution procedure and were refined by full-matrix least squares. In the final refinement, the non-hydrogen atoms were refined anisotropically. The hydrogen atoms were included in the structure factor calculations, but their parameters were not refined. The final discrepancy indices for the 6356 observed reflections were $R = 0.063$ and $R_w = 0.072$. The final difference map peaks (<1.47 e Å^{-3}) were near those of the tungsten and vanadium atoms.

$Na_2Cs_2[V_2W_4O_{19}]\cdot 6H_2O$ (IV). Of the 2750 independent reflections for $\theta < 75^o$, 2487 were considered observed [$I > 3.0\sigma(I)$]. The structures were solved by a multiple-solution procedure and were refined by full-matrix least squares. In the final refinement, the heavy atoms were refined anisotropically, and the oxygen atoms were refined isotropically. The final discrepancy indices were $R = 0.0444$ and $R_w = 0.0541$ for the 2487 observed reflections. The final difference map peaks (<2.10 e Å^{-3}) were near those of the tungsten and vanadium atoms.

Solution NMR Spectroscopy. ^{51}V and ^{183}W solution NMR spectra were acquired at 9.4 T on a JEOL GSX-400 spectrometer equipped with a Delta data system. The ^{51}V and ^{183}W resonance frequencies were 105.12 and 16.64 MHz, respectively. ^{51}V spectra were acquired using a 5 mm broadband probe; for ^{183}W spectroscopy, a 10 mm probe was utilized. ^{51}V spectra were acquired using a 5.8 μs (30°) single pulse; the ^{183}W spectra were acquired with a 50 μs (45°) single pulse. The ^{51}V spectra were acquired with 2048 complex FID points, a total acquisition time of 48.7 ms, and a recycle delay of 500 ms. The ^{183}W spectra were collected with 16384 complex FID points, a total acquisition time of 1.23 s, and a recycle delay of 500 ms. The spectra were processed with 2 and 10 Hz exponential linebroadening for ^{51}V and ^{183}W, respectively; no zero filling was applied. The isotropic chemical shifts are reported relative to that of the neat $VOCl_3$ sample, used as the referencing standard.

Solid-State NMR Spectroscopy. ^{51}V solid-state NMR spectra were acquired at 105.2 MHz (9.4 T) on a Tecmag Discovery spectrometer using a 4 mm Doty XC4 MAS probe. Spectra were recorded using 8−16 mg of sample. For each of the compounds, spectra at several different spinning speeds ranging between 4 and 17 kHz were acquired. The spinning speed was controlled to within ±5 Hz. The magic angle was adjusted using $NaNO_3$ (by detecting the ^{23}Na MAS signal), which yields an accuracy of ±0.005°. A single 1 μs pulse ($\gamma\mathscr{H}_1/2\pi \approx 80$ kHz) was employed to excite the central and the satellite transitions; 1 s recycle delays were used. The spectral widths were 1.25 MHz. A total of 4096 complex data points were acquired. The data were processed by linear prediction of the first 66 points to suppress the

(39) Skibsted, J.; Nielsen, N. C.; Bildsøe, H.; Jacobsen, H. J. *J. Magn. Reson.* **1991**, *95*, 88−117.
(40) Skibsted, J.; Jakobsen, H. J. *Inorg. Chem.* **1999**, *38*, 1806−1813.
(41) Jacobsen, H. J.; Skibsted, J.; Bildsøe, H.; Nielsen, N. C. *J. Magn. Reson.* **1989**, *85*, 173−180.
(42) Koller, H.; Engelhardt, G.; Kentgens, A. P. M.; Sauer, J. *J. Phys. Chem.* **1994**, *98*, 1544−1551.
(43) Marichal, C.; Kempf, J.-Y.; Maigret, B.; Hirschinger, J. *Solid State NMR* **1997**, *8*, 33−46.
(44) Bryant, P. L.; Harwell, C. R.; Wu, K.; Fronczek, F. R.; Hall, R. W.; Butler, L. G. *J. Phys. Chem. A* **1999**, *103*, 5246−5252.
(45) Moore, E. A.; Johnson, C.; Mortimer, M.; Wigglesworth, C. *Phys. Chem. Chem. Phys.* **2000**, *2*, 1325−1331.
(46) Tsvyashchenko, A. V.; Fomicheva, L. N.; Magnitskaya, M. V.; Shirani, E. N.; Brudanin, V. B.; Filossofov, D. V.; Kochetov, O. I.; Lebedev, N. A.; Novgorodov, A. F.; Salamatin, A. V.; Korolev, N. A.; Velichkov, A. I.; Timkin, V. V.; Menushenkov, A. P.; Kuznetsov, A. V.; Shabanov, V. M.; Akselrod, Z. Z. *Solid State Comm.* **2001**, *119*, 153−158.
(47) Blaha, P.; Schwartz, K.; Herzig, P. *Phys. Rev. Lett.* **1985**, *54*, 1192−1195.
(48) Bryce, D. L.; Wasylishen, R. E. *Phys. Chem. Chem. Phys.* **2002**, *4*, 3591−3600.
(49) Munro, O. Q.; Shabalala, S. C.; Brown, N. J. *Inorg. Chem.* **2001**, *40*, 3303−3317.
(50) Domaille, P. J. *J. Am. Chem. Soc.* **1984**, *106*, 7677−7687.

baseline distortions, followed by Fourier transformation and baseline correction using the MestRe-C23 NMR data processing software.[51] Isotropic chemical shifts are reported with respect to that of neat $VOCl_3$, whose ^{51}V spectrum was recorded and used as an external referencing standard.

Simulations of the NMR Spectra. Numerical simulations of the experimental ^{51}V solid-state NMR spectra were performed on a 1.1 GHz Pentium-4 PC under the Linux environment using the SIMPSON software package.[52] The combined effect of the quadrupolar interaction to second order and chemical shielding anisotropy was taken into account in the simulations. The seven independent parameters describing the quadrupolar and CSA tensor anisotropies (C_Q, η_Q, δ_σ, and η_σ) and the relative tensor orientations (the Euler angles α, β, and γ) were obtained by the least-squares fitting of the simulated and experimental sideband intensities using a home-written program under the Mathematica 4.1 (Wolfram, Inc.) environment. The quality factor of the probe (Q) has been taken into account in the simulations.

Calculations of Quadrupolar and Chemical Shielding Interaction Parameters. The quadrupolar coupling constant C_Q and the asymmetry parameter of the EFG tensor η_Q were calculated using a point monopole approximation according to refs 24 and 43. Mulliken charges were used on all the atoms except for the Na^+ and Cs^+ countercations, where the charges were assumed to be +1. The charges were calculated from natural population analysis using density functional theory for the bare $[VW_5O_{19}]^{3-}$ and $[V_2W_4O_{19}]^{4-}$ anions, and those complexed with tetramethylammonium cation; these calculations are reported elsewhere.[53] The central oxoanion together with the countercations in the first coordination sphere of the anion was used in the simulation. On the basis of the crystallographic coordinates and charges of each atom in the first coordination sphere, the matrix giving the electric field gradient at the central vanadium nucleus was calculated, with the nine entries $V_{ij} = ne(3ij/r^5 - \delta_{ij}/r^3)$, where e is the electronic charge, ne is the charge on each atom, i and j are the Cartesian x, y, or z coordinates of the ligand atom (assuming the coordinates of the central vanadium are (0, 0, 0)), and r is the distance between the ligand and the central vanadium atom. The matrices representing the individual contributions from each of the ligand atoms were subsequently summed up, and the resulting tensor was diagonalized to obtain its principal components. The largest principal value $V_{zz} = eq$ was used to calculate the quadrupolar coupling constant $C_Q = (1 - \gamma_\infty)(e^2qQ/h)$, where γ_∞ is the Sternheimer antishielding factor[54] (−7.6 for ^{51}V).[35]

The asymmetry parameter of the electric field gradient was calculated from the principal components of the EFG tensor according to the definition in the previous section. The calculations were performed using a PC home program written under the Mathematica environment; the program is available at http://patsy.hunter.cuny.edu/FandS/TP/MATHEMATICA/Quadrupolar_tensor_calculation.nb. Since it is only the absolute magnitude of the quadrupolar interaction that can be measured by NMR, the signs of the calculated quadrupolar tensor are omitted.

Results and Discussion

Spectroscopic Characterization of the Six-Coordinate Oxoanions I−IV. We have acquired IR (solid, KBr pellets) and multinuclear (^{183}W and ^{51}V) solution NMR spectra for the four mono- and divanadium-substituted hexatungstates under investigation. The IR spectra and solution NMR chemical shifts are in good agreement with the previously reported data.[50,55,56] ^{183}W solution NMR spectra confirm the cis-configuration of the $[V_2W_4O_{19}]^{4-}$ anion, in agreement with the previous assignments.[50,57]

The IR frequencies and solution NMR isotropic chemical shifts are deposited as Supporting Information. More detailed discussion about the effect of the nature of the countercation and the presence of hydration waters on the infrared frequencies of vanadium-substituted hexatungstates is presented elsewhere.[53]

Single-Crystal X-ray Diffraction of I and III. The *n*-tetrabutylammonium salts of mono- and divanadium-substituted hexatungstates crystallize in a monoclinic *C*2/*c* space group, with eight oxoanion molecules per unit cell. The crystal data and structure refinement parameters are given in Table 1. The CIF files containing the crystallographic coordinates for these structures are deposited as Supporting Information.

The overall structures of the oxoanions in **I** and **III** are consistent with those reported previously for similar mono- and divanadium hexatungstates, $[N(CH_3)_4]_2(NH_4)[VW_5O_{19}]$ and $(CN_3H_6)_4[V_2W_4O_{19}]$.[55,58] Positional disorder with respect to the vanadium atom(s) is present in the structures, which is quite common for the substituted heteropoly anions.[55,58,59] The X-ray data can be explained assuming random orientation of vanadium atoms in the tungstate framework. The stoichiometry of substituted heteropoly anions in the X-ray crystal structures can only be inferred from the relative site occupancies, and this kind of analysis is intrinsically associated with large errors. For example, the structure of **III** refined to relative W:V occupancies of 2:1 in agreement with the stoichiometry. The structure of **I** could be equally well refined with occupancies of either 5:1 or 2:1, indicating either 1 or 2 vanadium atoms could be present in the crystal. However, solution NMR, solid-state NMR, and IR data clearly indicate one vanadium to be present per molecule of **I**, in agreement with the $[VW_5O_{19}]^{3-}$ molecular formula. These spectroscopic data indicate two vanadium atoms per molecule of **III**, in agreement with the $[V_2W_4O_{19}]^{4-}$ formula.

The crystal structure of **III** reveals only three *n*-tetrabutylammonium countercations present per $[V_2W_4O_{19}]^{4-}$ anion. Electron densities corresponding only to the oxoanion and to the three $[(n\text{-}C_4H_9)_4N]^+$ cations could be identified. We therefore concluded that an additional H^+ is likely to be present in the structure to balance the overall charge of the anion. This is also consistent with the fact that **III** was prepared under acidic conditions (pH 2.0).

Figure 1 depicts the $[VW_5O_{19}]^{3-}$ anions within the unit cell of **I** (a), and the coordination environment for a single $[VW_5O_{19}]^{3-}$ anion (b). In Figure 2, the corresponding information for **III** is presented. The coordination environments of the oxoanions in these two compounds are very similar; the effect of the environment on the ^{51}V solid-state NMR spectra will be discussed in the following sections.

Single-Crystal X-ray Diffraction of IV. The mixed Na^+/Cs^+ salt of divanadium oxotungstate crystallizes in a triclinic

(51) Cobas, J.; Cruces, J.; Sardina, F. J. *MestRe-C: Magnetic Resonance Companion*; Departamento de Quimica Organica, Facultat de Quimica, Universidad de Santiago de Compostela: Santiago de Compostela, Spain, 2000.
(52) Bak, M.; Rasmussen, J. T.; Nielsen, N. C. *J. Magn. Reson.* **2000**, *147*, 296−330.
(53) Dmitrenko, O. G.; Huang, W.; Polenova, T.; Francesconi, L. C. Accepted for publication in *J. Phys. Chem. B.*
(54) Beri, A. C.; Lee, T.; Das, T. P.; Sternheimer, R. M. *Phys. Rev. B* **1983**, *28*, 2335−2351.
(55) Klevtsova, R. F.; Yurchenko, E. N.; Glinskaya, L. A.; Derkach, I. V.; Markes-Rios, A. *J. Struct. Chem.* **1988**, *29*, 418−421.
(56) Flynn, C. M.; Pope, M. T. *Inorg. Chem.* **1971**, *10*, 2524−2529.
(57) Klemperer, W. G.; Shum, W. *J. Am. Chem. Soc.* **1978**, *100*, 4891−4893.
(58) Nishikawa, K.; Kobayashi, A.; Sasaki, Y. *Bull. Chem. Soc. Jpn.* **1975**, *48*, 889−892.
(59) Luo, Q.-H.; Howell, R.; Dankova, M.; Bartis, J.; Williams, C. W.; Horrocks, W. D. J.; Young, V. G. J.; Rheingold, A. L.; Francesconi, L. C.; Antonio, M. R. *Inorg. Chem.* **2001**, *40*, 1894−1901.

Table 1. Crystal Data and Structure Refinement for $[(n\text{-}C_4H_9)_4N]_3[VW_5O_{19}]$, $[(n\text{-}C_4H_9)_4N]_3H[V_2W_4O_{19}]$, and $Na_2Cs_2[V_2W_4O_{19}]\cdot 6H_2O$

	$[(n\text{-}C_4H_9)_4N]_3[VW_5O_{19}]$	$[(n\text{-}C_4H_9)_4N]_3H[V_2W_4O_{19}]$	$Na_2Cs_2[V_2W_4O_{19}]\cdot 6H_2O$
empirical formula	$C_{48}H_{108}N_3VW_5O_{19}$	$C_{48}H_{108}N_3V_2W_4O_{19}$	$Na_2Cs_2V_2W_4O_{19}\cdot 6H_2O$
FW	2001.536	1868.637	1561.154
temp (K)	295	295	295
cryst syst	monoclinic	monoclinic	triclinic
space group	*C*2/*c*	*C*2/*c*	*P*1
a (Å)	30.090(6)	30.135(7)	8.546(1)
b (Å)	18.390(3)	18.377(2)	8.550(1)
c (Å)	31.967(6)	27.279(4)	11.194(1)
α (deg)	90	90	67.59(1)
β (deg)	128.10(2)	112.40(2)	67.63(1)
γ (deg)	90	90	59.99(1)
V (Å^3)	13919.8(55)	13966.9(46)	636.0(2)
D_x (g/cm^3)	1.910	1.777	4.076
Z	8	8	1
μ(Cu Kα) (cm^{-1})	166.30	165.74	616.46
cryst size (mm)	0.05 × 0.16 × 0.25	0.12 × 0.36 × 0.40	0.07 × 0.14 × 0.14
max θ for data collection (deg)	60	60	75
no. of reflns collected/unique	10328/7289	10364/6356	2750/2487
refinement method	full-matrix least squares on F^2	full-matrix least squares on F^2	full-matrix least squares on F^2
no. of variables	450	453	196
min/max transm (%)		1.72/23.07	1.57/14.4
R	0.078	0.063	0.052
R_w	0.094	0.072	0.0684
largest diff peak and hole, e/Å^3	1.57 and 2.80	1.47 and −1.44	1.83 and 2.10

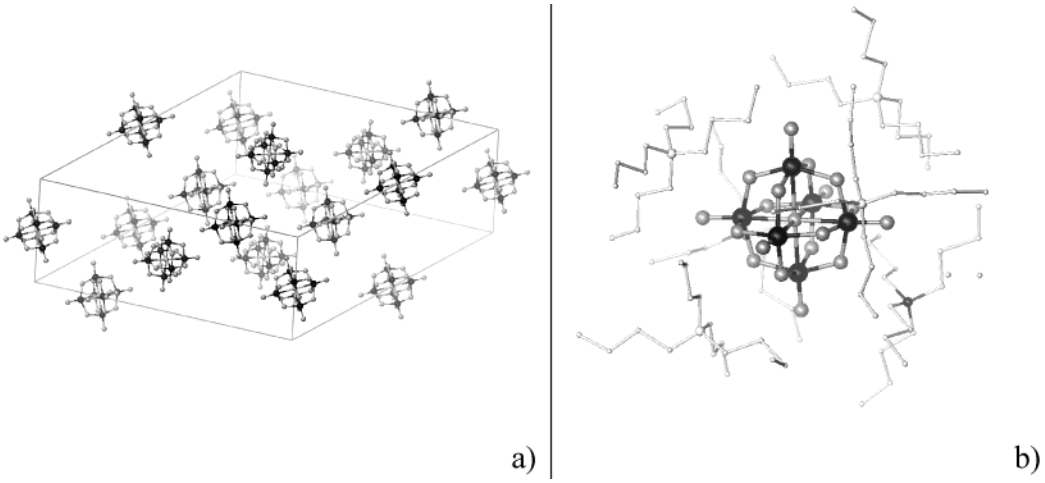

Figure 1. (a) Unit cell of $[(n\text{-}C_4H_9)_4N]_3[VW_5O_{19}]$. The *n*-tetrabutylammonium countercations are omitted for clarity. Vanadium atoms display positional disorder within the crystal lattice. (b) Cationic environment in the crystal for a single $[VW_5O_{19}]^{3-}$ anion. Each anion is surrounded by six cation molecules. The molecules are depicted in a ball-and-stick representation. In the anion, W atoms are depicted with dark gray color, and O atoms are smaller spheres shown in lighter gray. In the TBA cation molecules, the N atoms are depicted as bigger spheres. H atoms are omitted.

*P*1 space group. The crystal data and structure refinement parameters are given in Table 1. The CIF file containing the crystallographic coordinates for this molecule is deposited as Supporting Information.

Similar to **I** and **III**, positional disorder with respect to the vanadium atoms is observed in the structure. The structure was refined assuming random orientation of the vanadium atoms in the oxoanion framework, with relative W:V occupancies of 2:1, in agreement with the stoichiometry.

All four monovalent cations required for neutrality were found in the crystal structure: two Na^+ cations and two Cs^+ cations. In addition, six molecules of hydration water are present in the crystal structure; these are ordered according to the well-defined electron densities of the oxygen atoms.

Figure 3 depicts the $V_2W_4O_{19}^{4-}$ anions within the unit cell of **IV** (a), and the first coordination sphere environment for a single $[V_2W_4O_{19}]^{4-}$ anion (b). Curiously, the crystal structure reveals that the divanadium tungstates are sandwiched between layers of Na^+/Cs^+ countercations and hydration water, as shown in Figure 4. The electrostatic environment of the anion thus appears to differ significantly from the environment in the corresponding *n*-tetrabutylammonium complex. The effect of the electrostatic environment of the ^{51}V solid-state NMR spectra will be addressed in the following discussion.

^{51}V Solid-State NMR Magic Angle Spinning Spectroscopy: Isotropic Chemical Shifts and Anisotropic Lineshapes. The ^{51}V MAS solid-state NMR spectra of **I**−**IV** at 8 kHz are presented in Figure 5. Both mono- and divanadium compounds display a single set of spinning sidebands, corresponding to one isotropic chemical shift, in agreement with the symmetry of the oxoanions. The isotropic chemical shifts are compiled in Table 2. The second-order quadrupole-induced shifts were taken into account as a correction to the experimentally observed isotropic sideband according to ref 60:

(60) Kundla, E.; Samoson, A.; Lipmaa, E. *Chem. Phys. Lett.* **1981**, *83*, 229.

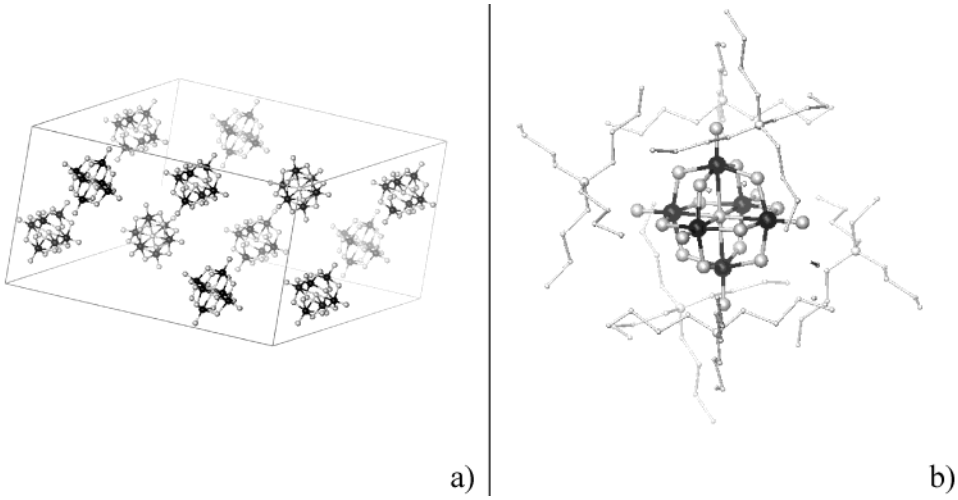

Figure 2. (a) Unit cell of $[(n\text{-}C_4H_9)_4N]_3H[V_2W_4O_{19}]$. The *n*-tetrabutylammonium countercations are omitted for clarity. Vanadium atoms display positional disorder within the crystal lattice. (b) Cationic environment in the crystal for a single $[V_2W_4O_{19}]^{4-}$ anion. Each anion is surrounded by six cation molecules. An additional H^+ cation is likely to be present in the structure for charge neutrality; however, it is not revealed in the electron density, and is thus not shown here. The molecules are depicted in a ball-and-stick representation. In the anion, W atoms are depicted with dark gray color, an O atoms are smaller spheres shown in lighter gray. In the TBA cation molecule, the N atom is depicted as a bigger sphere. H atoms are omitted.

Table 2. Experimental ^{51}V Solid-State NMR Parameters for the Vanadium-Substituted Hexatungstates **I**−**IV**: ^{51}V Isotropic Chemical Shifts (δ_{iso}), Quadrupolar Couplings (C_Q, η_Q), Chemical Shielding Anisotropies (δ_σ, η_σ), and the Euler Angles (α, β, γ) Describing the Relative Orientations of the Two Tensors

compd	C_Q (MHz)	η_Q	δ_σ (ppm)	η_σ	α (deg)	β (deg)	γ (deg)	δ_{obsd} (ppm) (solid state)	quadrupole-induced shift (ppm)	δ_{iso} (ppm) (solid state)	δ_{iso} (ppm) (soln)
I	0.605 ± 0.005	0.65 ± 0.05	199.5 ± 9.5	0.95 ± 0.05	90 ± 5	30 ± 5	0 ± 5	−504.9	−0.1	−504.8	−510.0
II	1.3 ± 0.005	0.8 ± 0.1	465.8 ± 9.5	0.10 ± 0.10	70 ± 10	0 ± 5	40 ± 10	−520.0	−0.39	−519.6 1	insoluble
III	1.05 ± 0.05	0.95 ± 0.05	418.2 ± 9.5	0.10 ± 0.05	70 ± 10	0 ± 5	50 ± 15	−505.5	−0.25	−505.2 5	−509.5
IV	1.555 ± 0.005	0.35 ± 0.05	456.3 ± 9.5	0.2 ± 0.05	80 ± 5	60 ± 5	50 ± 5	−526.6	−0.6	−526.0	−512.0,[a] −526[b]

[a] pH 5.5. [b] pH 2.0.

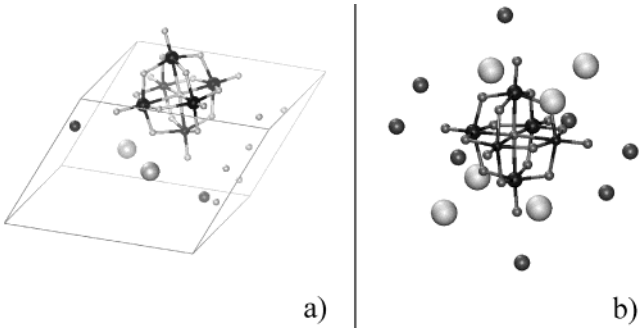

Figure 3. (a) Unit cell of $Na_2Cs_2[V_2W_4O_{19}]\cdot 6H_2O$. Vanadium atoms display positional disorder within the crystal lattice. (b) Arrangement of cations and solvent water molecules for a single $[V_2W_4O_{19}]^{4-}$ anion. The molecules are depicted in a ball-and-stick representation. In the anion, W atoms are depicted with dark gray color, V atoms are smaller dark gray spheres, and O atoms are the smallest spheres shown in lighter gray. The countercation atoms are depicted as follows: Cs^+ ions are the largest light spheres, and Na^+ atoms are the smaller darker gray spheres.

$$\delta_{obsd} - \delta_{iso} = \frac{(-3 \times 10^6)(e^2qQ/h)^2[I(I+1) - 9m(m-1) - 3][1 + \eta^2/3]}{40(\nu_0^{\,2})[I(2I-1)]^2} \quad (6)$$

where e^2qQ/h is the quadrupolar coupling constant (MHz), I is the spin number ($I = 7/2$ for ^{51}V), m is the magnetic spin number ($m = 1/2$ for the central transition), η is the asymmetry of the CSA tensor, and ν_0 is the resonance frequency of the ^{51}V nucleus (105.2 MHz at 9.4 T). For the compounds reported in this work, these upfield shifts were small and ranged from −0.1 to −0.6 ppm.

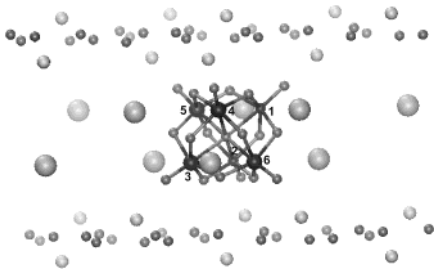

Figure 4. Crystal environment of $[V_2W_4O_{19}]^{4-}$ in $Na_2Cs_2[V_2W_4O_{19}]\cdot 6H_2O$ beyond the immediate neighboring cations and hydration water molecules. The oxoanions are sandwiched between the Na^+/Cs^+ countercations and the hydration water molecules. Thus, the electrostatic environment of the oxoanion is very different from that in the $[(n\text{-}C_4H_9)_4N]^+$-coordinated complex. ^{51}V solid-state NMR spectroscopy is very sensitive to these differences; the experimental parameters describing the quadrupolar and chemical shielding anisotropies are in good agreement with the geometric structure when the countercations are taken into account. The molecules are depicted in a ball-and-stick representation. In the anion, W atoms are depicted with dark gray color, V atoms are smaller dark gray spheres, and O atoms are the smallest spheres shown in lighter gray. The countercation atoms are depicted as follows: Cs^+ ions are the largest light spheres, and Na^+ atoms are the smaller darker gray spheres.

The ^{51}V solution and solid-state isotropic chemical shifts differ by several parts per million, suggesting the local environment of the vanadium nucleus changes in the solid state. The pH of the sample has the largest effect on the isotropic shifts in

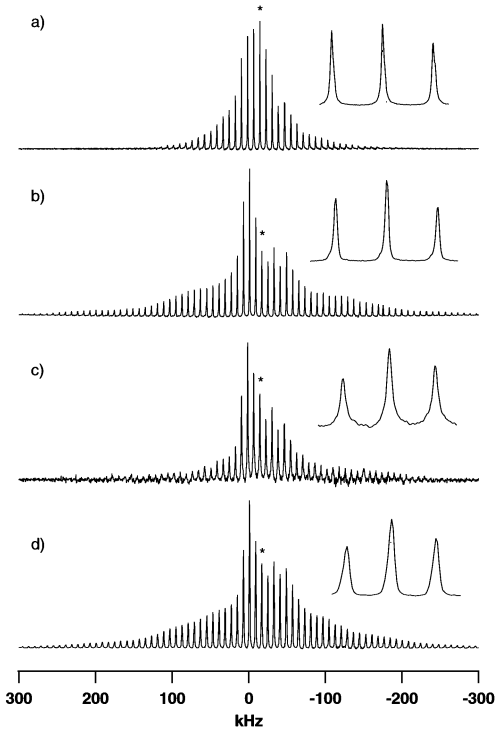

Figure 5. Experimental ^{51}V MAS NMR spectra of (a) **I**, (b) **II**, (c) **III**, and (d) **IV** at 8 kHz. The center band is indicated with an asterisk. The isotropic chemical shifts are compiled in Table 2 with respect to that of neat $VOCl_3$, used as an external referencing standard. For **I**, **III**, and **IV**, the spectra were collected for microcrystalline samples (not shown) and diffraction-quality crystals, and are essentially indistinguishable. The insets are expansions around the centerband to demonstrate the lineshapes of the individual spinning sidebands (insets are not to scale).

solution, where discrepancies as large as 15 ppm are observed for different conditions (Table 1s in the Supporting Information).

In the solid state, the isotropic chemical shifts appear to be in large determined by the nature of the countercation. In **I** and **III**, which are complexed with a TBA countercation, the vanadium atoms are more deshielded, with isotropic chemical shifts of −504.9 and −505.5 ppm, respectively. The corresponding chemical shifts for **II** and **IV**, whose countercations are alkali metals, are −520.0 and −526.6 ppm, respectively. Interestingly, for **I**, **III**, and **IV** the isotropic chemical shifts in solution at the same pH are very similar (**II** is insoluble, and its solution NMR spectrum could not be acquired), thus attesting to the dominating influence of the countercation on the solid-state isotropic chemical shifts. The electric field gradient tensor is also determined by the countercation (vide infra).

Asymmetric spectral envelopes observed for all compounds indicate large chemical shielding anisotropies. The overall width of the spectral envelope reflects the magnitude of the quadrupolar interaction, and varies significantly among this series. The quadrupolar anisotropy is the largest in the mono- and divanadium tungstates **II** and **IV** complexed with Na^+/Cs^+, suggesting a more asymmetric charge distribution in these solids. The spectra appear to be very sensitive to the details of the local environment at the vanadium site, as will be discussed in the following sections.

Solid-State NMR Spectral Linewidths. The insets in Figures 5−9 contrast the lineshapes for the individual spinning sidebands. The linewidths range between 5.8 and 11.6 ppm. There are several possible contributions to the linewidths, namely, the second-order quadrupolar broadening, the positional disorder in vanadium distribution, the dipolar broadening, and the bulk morphology of the solid.

The second-order quadrupolar term has a relatively weak effect on the linewidths of **I** and **III** due to the small quadrupolar coupling constants in these solids (vide infra, Table 2). In **II** and **IV** the coupling constants are larger (Table 2), and we expected a more pronounced contribution from this term. Indeed, experimental sidebands in **II** and **IV** were broader than in **I** and **III**, and the simulated spectra revealed the characteristic second-order quadrupolar lineshape (insets in Figures 7 and 9).

Positional disorder with respect to the vanadium atoms revealed in the crystal structures of **I**, **III**, and **IV** (vide supra), and expected to be present in **II** as well, will introduce additional linebroadening. This is a result of the spread in the quadrupolar coupling constant values arising due to this disorder, as suggested by the electrostatic calculations for **IV** (vide infra, Table 3).

Interestingly, the lines are consistently broader for the divanadium **III** and **IV** anions regardless of the nature of the countercation, suggesting a homonuclear ^{51}V−^{51}V dipolar interaction to introduce additional broadening in the individual spinning sidebands. The V−V distance in the *cis*-divanadium tungstate is 3.2 Å, and the corresponding dipolar coupling constant ω_D is 250 Hz. Additionally, as has been pointed out by S. Wimperis and colleagues previously,[61] in a dipolar-coupled system of two quadrupolar nuclei, such as a ^{51}V−^{51}V pair, a second-order quadrupolar−dipolar cross term is not averaged out by MAS, resulting in additional broadening of the spinning sidebands. However, since this term is scaled with the quadrupolar coupling strength,[61] its contribution to the linewidth is expected to be insignificant (on the order of 15−30 Hz) for the compounds discussed in this work.

It is quite common for the bulk morphology of the sample to affect the NMR linewidths in solid systems.[23,41] ^{51}V solid-state NMR linewidths could potentially serve as an indicator of the degree of crystallinity in the solid sample. For the Lindqvist compounds addressed in this study we found the linewidths to be very similar for the samples prepared as powders and diffraction-quality crystals, suggesting a significant degree of microcrystallinity in the powder samples. Indeed, powder X-ray diffraction measurements of **I**−**IV** confirm the solid-state NMR observations indicating that all of the powder samples are microcrystalline and not amorphous solids. To date we have not been able to prepare an amorphous powder sample to compare the linewidths with those for the crystalline samples; this work is currently in progress.

Simulations of the Solid-State NMR Spectra. The parameters describing the quadrupolar and CSA interactions were determined from numerical simulations of the solid-state NMR spectra and are reported in Table 2 for each of the four compounds. The asymmetric lineshapes in the MAS spectra are a result of the combined effect of the anisotropic quadrupolar and CSA interactions, and are in turn described by seven independent parameters: the anisotropy and the asymmetry of the quadrupolar and CSA tensors (C_Q, η_Q, δ_σ, and η_σ), and the three Euler angles (α, β, and γ) relating the principal axes

(61) McManus, J.; Kemp-Harper, R.; Wimperis, S. *Chem. Phys. Lett.* **1999**, *311*, 292−298.

Table 3. Quadrupolar Interaction Parameters for the Crystallographically Characterized Compounds **I**, **III**, and **IV** Calculated from the Electrostatic Model

compd	C_Q (MHz) (exptl)	η_Q (exptl)	C_Q (MHz) (calcd)	η_Q (calcd)	central vanadium atom[b]	neighboring vanadium atom[b]
$VW_5O_{19}^{3-}$			0.079[a]	0.01[a]		
I	0.605 ± 0.005	0.65 ± 0.05	0.268	0.53		
III	1.05 ± 0.05	0.95 ± 0.05	0.295	0.43		
IV	1.555 ± 0.005	0.35 ± 0.05	0.869 ± 0.254[c]	0.67 ± 0.20[c]		
			0.767	0.85	1	2
			0.636	0.47	1	4
			0.667	0.75	1	5
			0.883	0.64	1	6
			0.849	0.84	2	1
			1.08	0.42	2	3
			0.876	0.62	2	5
			1.03	0.38	2	6
			1.19	0.99	3	2
			1.19	0.57	3	4
			1.03	0.96	3	5
			1.06	0.99	3	6
			0.690	0.96	4	1
			0.828	0.74	4	3
			0.741	0.59	4	5
			0.861	0.95	4	6
			0.374	0.72	5	1
			0.534	0.83	5	2
			0.677	0.62	5	3
			0.426	0.94	5	4
			1.15	0.31	6	1
			1.20	0.37	6	2
			1.24	0.29	6	3
			1.20	0.42	6	4

[a] Calculation for the "bare" $VW_5O_{19}^{3-}$ using NBO charges for the oxygen atoms. [b] Numbering of vanadium atoms according to Figure 4. The vanadium atoms could not be identified from the X-ray structure. They were assumed to adopt random positions in the crystal while preserving the overall cis-configuration of the oxoanion molecule, as was also confirmed by ^{51}V solution NMR data (see the text). The quadrupolar tensor parameters were then calculated for each possible orientation of the vanadium pair in the structure. [c] Mean values and standard deviations.

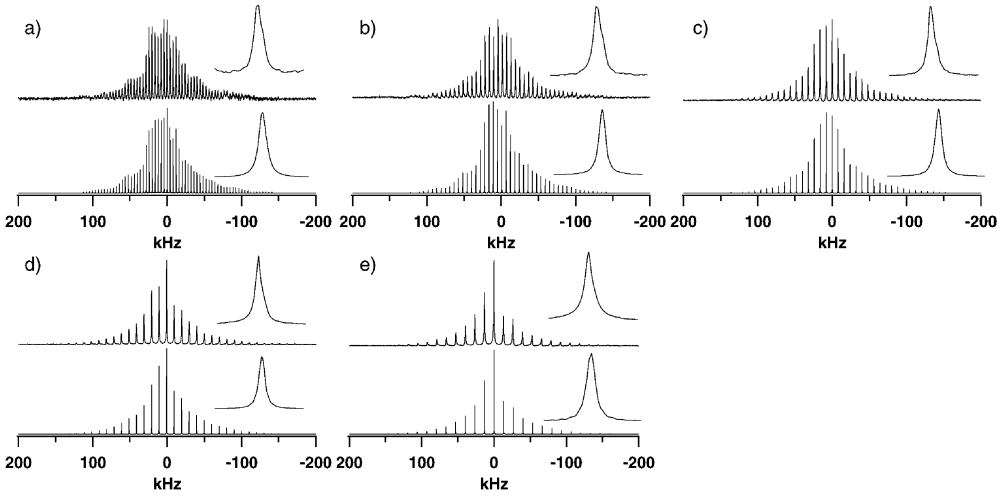

Figure 6. Experimental (top) and simulated (bottom) ^{51}V MAS NMR spectra of **I** at (a) 4.020 kHz, (b) 5.841 kHz, (c) 8.012 kHz, (d) 10.081 kHz, and (e) 13.298 kHz. The spectra were simulated using the following parameters: $C_Q = 0.605 \pm 0.005$ MHz; $\delta_\sigma = 199.5 \pm 9.5$ ppm; $\eta_Q = 0.65 \pm 0.05$; $\eta_\sigma = 0.95 \pm 0.05$; $\alpha = 90 \pm 5°$; $\beta = 30 \pm 5°$; $\gamma = 0 \pm 5°$. The rmsd values were (a) 0.08, (b) 0.08, (c) 0.05, (d) 0.04, and (e) 0.04. The horizontal scale is in kilohertz to illustrate the overall widths of the quadrupolar tensor. The insets are expansions of a satellite peak comparing the experimental and simulated lineshapes of the individual spinning sidebands.

system of the quadrupolar and CSA tensors. For ^{51}V and a number of half-integer quadrupolar nuclei, the quadrupolar and CSA interactions are orders of magnitude different in strength, thus allowing for the seven independent parameters describing these interactions to be obtained from a single MAS spectrum.

We have acquired and simulated MAS spectra for each compound at five different spinning speeds, to be able to extract with greater accuracy the quadrupolar and CSA tensor elements, and to obtain reliable error estimates.

In Figures 6−9, the experimental and simulated spectra are presented for **I**−**IV**. The quadrupolar coupling constants for compounds **II** and **IV** are 1.300−1.555 MHz, as compared with 0.650 and 1.050 MHz for **I** and **III**. There is a good general agreement in the resulting anisotropic observables at all spinning speeds. However, at spinning speeds higher than 10 kHz for **I**, the calculated asymmetry of the chemical shielding tensor deviates significantly from the values obtained at lower speeds. As was discussed previously, measurements at sufficiently high

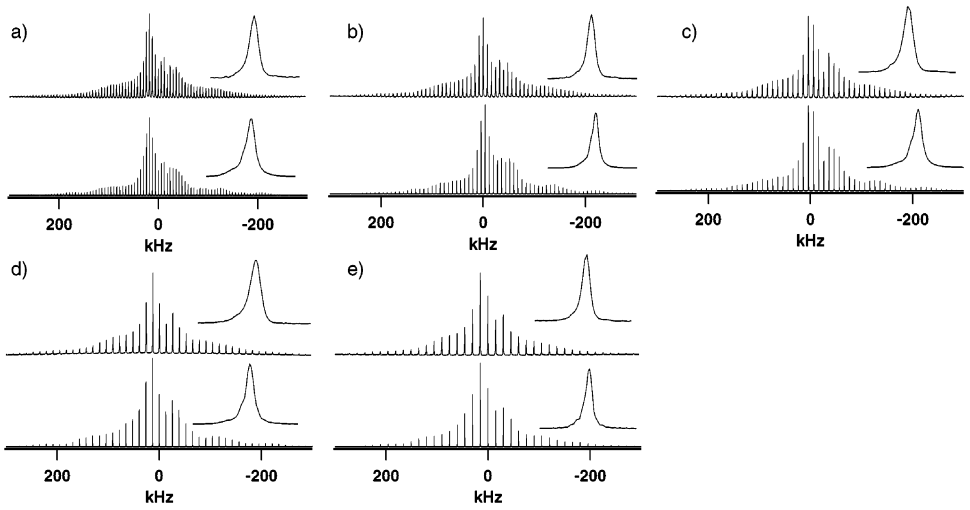

Figure 7. Experimental (top) and simulated (bottom) ^{51}V MAS NMR spectra of **II** at (a) 5.968 kHz, (b) 8.005 kHz, (c) 10.000 kHz, (d) 13.010 kHz, and (e) 15.048 kHz. The spectra were simulated using the following parameters: $C_Q = 1.30 \pm 0.05$ MHz; $\delta_\sigma = 465.8 \pm 9.5$ ppm; $\eta_Q = 0.8 \pm 0.1$; $\eta_\sigma = 0.10 \pm 0.10$; $\alpha = 70 \pm 10°$; $\beta = 0 \pm 5°$; $\gamma = 40 \pm 10°$. The rmsd values were (a) 0.07, (b) 0.07, (c) 0.07, (d) 0.09, and (e) 0.06. The insets are expansions of a satellite peak comparing the experimental and simulated lineshapes of the individual spinning sidebands.

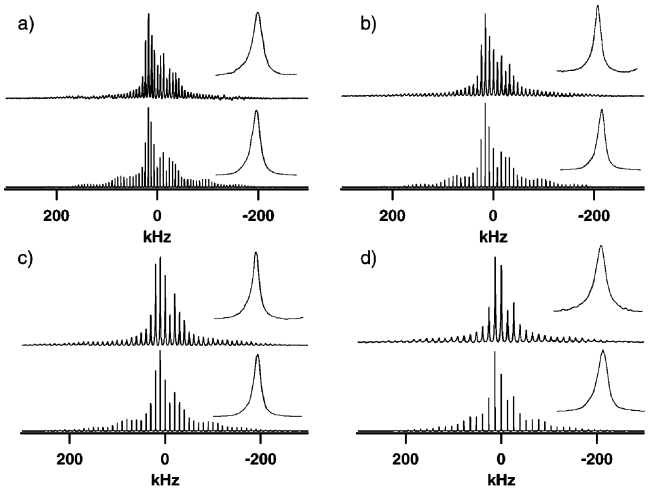

Figure 8. Experimental (top) and simulated (bottom) ^{51}V MAS NMR spectra of **III** at (a) 5.996 kHz, (b) 8.005 kHz, (c) 10.000 kHz, and (d) 13.000 kHz. The spectra were simulated using the following parameters: $C_Q = 1.05 \pm 0.05$ MHz; $\delta_\sigma = 418.2 \pm 9.5$ ppm; $\eta_Q = 0.95 \pm 0.10$; $\eta_\sigma = 0.10 \pm 0.05$; $\alpha = 70 \pm 10°$; $\beta = 0 \pm 5°$; $\gamma = 50 \pm 15°$. The rmsd values were (a) 0.15, (b) 0.11, (c) 0.11, and (d) 0.11. The insets are expansions of a satellite peak comparing the experimental and simulated lineshapes of the individual spinning sidebands.

spinning speeds (determined by the magnitude of the largest anisotropic interaction in the system) are expected to yield inaccurate estimates for the anisotropic observables.[62] In **I**, the relatively weak quadrupolar interaction determines the upper bound of the spinning speed, at which the anisotropic observables can be extracted with a sufficient degree of accuracy. At 10 and 13 kHz, it is only the asymmetry of the CSA tensor that differs from the lower spinning speed estimates, in agreement with the expected behavior.[62]

Electrostatic Calculations of the EFG and Quadrupolar Tensors. Experimental data indicate that the anisotropic ^{51}V quadrupolar interaction in **I**−**IV** is in large dictated by the nature and geometry of the countercations in the crystal lattice. The quadrupolar interaction reflects the electrostatic environment around the nucleus, and for the compounds described in this work it appears to be a very sensitive probe for the charge geometry around the polyoxoanion. On the basis of the crystal structures of **I**, **III**, and **IV**, we have calculated the quadrupolar interaction parameters assuming a point monopole model.[22,24,63] The results are compiled in Table 3. For the "bare" $VW_5O_{19}^{3-}$ anion where the local symmetry of the vanadium nucleus is formally distorted octahedral, the strength of the quadrupolar interaction according to the calculation is small (ca. 79 kHz). The predicted asymmetry parameter is close to 0, as expected. In **I** and **III**, the presence of tetrabutylammonium cations appears to affect both the strength of the quadrupolar interaction and the asymmetry parameter according to the calculation. The coupling constant increases to ca. 270−300 kHz, and the asymmetry parameter to ca. 0.43−0.53. Experimental data for **I** and **III** indeed display a relatively small quadrupolar interaction (650 kHz and 1.050 MHz) and significant rhombicity ($\eta_Q = 0.65$ and 0.95).

The crystal structure of **IV** revealed that cations and hydration waters form layers with the oxoanion sandwiched between (vide supra), resulting in a different charge distribution as compared with **I** and **III**. Moreover, in **IV** the symmetry of the charge distribution appears to have a different effect on the quadrupolar tensors of the vanadium atoms depending on their position in the crystal structure. Since the vanadium atoms could not be identified from the X-ray structure, they were assumed to adopt random positions in the crystal while preserving the overall cis-configuration of the oxoanion molecule, as was also confirmed by ^{51}V solution NMR data (vide supra). The quadrupolar tensor parameters were then calculated for each possible orientation of the vanadium pair in the structure (Table 3). The magnitudes of the quadrupolar coupling constants resulting from this calculation range between 374 kHz and 1.24 MHz, with a mean value of 869 kHz and a standard deviation of 254 kHz. The calculated asymmetry parameter is 0.67 ± 0.20. Despite the spread of values, the general experimental trends are well reproduced; namely, the magnitude of the mean value for **IV** appears to be ca. 1.5−3-fold greater than for **III** and **I**, respectively.

(62) Hodgkinson, P.; Emsley, L. *J. Chem. Phys.* **1997**, *107*, 4808−4816.

(63) Koller, H.; Engelhardt, G.; Kentgens, A. P. M.; Sauer, J. *J. Phys. Chem.* **1994**, *98*, 1544−1551.

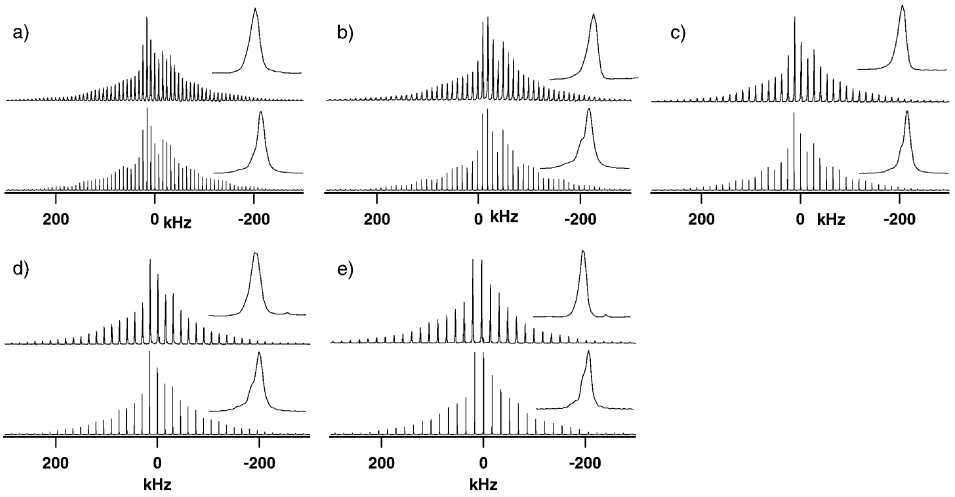

Figure 9. Experimental (top) and simulated (bottom) ^{51}V MAS NMR spectra of **IV** at (a) 7.983 kHz, (b) 9.983 kHz, (c) 13.093 kHz, (d) 15.080 kHz, and (e) 17.003 kHz. The spectra were simulated using the following parameters: $C_Q = 1.555 \pm 0.005$ MHz; $\delta_\sigma = 456.3 \pm 9.5$ ppm; $\eta_Q = 0.35 \pm 0.05$; $\eta_\sigma = 0.2 \pm 0.05$; $\alpha = 80 \pm 5°$; $\beta = 60 \pm 5°$; $\gamma = 50 \pm 5°$. The rmsd values were (a) 0.06, (b) 0.06, (c) 0.04, (d) 0.05, and (e) 0.05. The insets are expansions of a satellite peak comparing the experimental and simulated lineshapes of the individual spinning sidebands.

In the absence of an X-ray structure for **II**, the electrostatic calculations for the EFG and quadrupolar tensors could not be undertaken. However, the experimentally observed quadrupolar and CSA tensors are very close to those in **IV**, indicating that the crystal packings of **II** and **IV** are probably also similar. Moreover, the similarity of the X-ray structures of **I** and **III** suggests that the crystal packing may not be dependent on the number of vanadium atoms in the oxotungstate anion when the same countercation is used at similar conditions to form the polyoxometalate solid. The ^{51}V MAS spectra thus appear to be a sensitive probe of the electrostatic environment of the oxoanion.

The electrostatic model utilized in this work is an oversimplification, and cannot be applied for quantitative determination of the quadrupolar interaction parameters. It does however appear to reflect the overall trends in the magnitudes of the quadrupolar coupling constants in homologous series of compounds, especially those with ionic bond character, as has been demonstrated previously[22−24,63] and in this work. The model also accounts for the cation effect on the quadrupolar interaction parameters.

To obtain reliable estimates of the EFG and quadrupolar tensors, more rigorous quantum mechanical calculations are necessary. In recent years, density functional theory (DFT) has been increasingly used for computing the electric field gradients in solids, encompassing both cluster[45,48,49] and extended periodic treatments.[43−47,64] For heteropoly systems discussed in this work, we have not performed the calculations yet due to the extensive CPU time requirements. Since the effect of the countercations has to be considered, the smallest system would include 75−100 atoms per cluster or periodic cell, with a substantial number of heavy atoms. Work is in progress on establishing these calculations in our laboratory.

Effect of the Cationic Environment on Quadrupolar and CSA Tensors. The experimental data discussed above reveal that the anisotropic NMR observables (C_Q, δ_{iso}, and δ_σ) in vanadium hexatungstate solids under investigation are in large dictated by the nature and geometry of the countercations. The NMR parameters are similar within each series of solids complexed with TBA (**I** and **III**) and alkali-metal cations (**II** and **IV**) (Table 2). Substituting the second vanadium atom in the cis-position has a much weaker effect, influencing mostly δ_σ in **III**, and introducing additional dipolar broadening of individual spinning sidebands in **III** and **IV**.

It has been previously reported that countercations have an immediate effect both on the three-dimensional structure[10] and on the resulting physicochemical properties of POM solids.[11] Our study demonstrates that countercations modulate the electronic environment of the oxoanion, suggesting this to be a plausible explanation for the altered chemical reactivity of POMs in the solid state. Moreover, the ^{51}V solid-state NMR signatures of the hexametalates can potentially serve as benchmarks in designing materials with tunable structural and electronic properties for multiple applications.

Conclusions

We have addressed the influence of the cationic environment and number of vanadium atoms in the oxotungstate anion core on the ^{51}V MAS spectra of vanadium-substituted six-coordinate polyoxotungstates. The countercation has profound influence on the electronic properties of the oxoanion, which can be inferred from the ^{51}V chemical shielding and quadrupolar tensors experimentally measured by solid-state NMR. The linewidths of the individual spinning sidebands depend on the number of vanadium atoms in the anion. The ^{51}V quadrupolar tensor parameters calculated assuming the electrostatic model show good agreement with the experimental trends. Thus, ^{51}V magic angle spinning NMR spectroscopy is a sensitive probe of the geometric and electronic environment in polyoxometalate solids, and exhibits excellent promise to become a widely utilized technique for the analysis of POM materials.

Acknowledgment. We thank Professor Robert Beer of Fordham University for valuable discussions, and Professor Steve Greenbaum of Hunter College for instrument time at 7.1 T for the preliminary measurements. We thank Prof. Niels Chr. Nielsen and co-workers for the SIMPSON program. T.P. gratefully acknowledges the financial support of Hunter College,

(64) Schwarz, K.; Blaha, P. *Lect. Notes Chem.* **1996**, *67*, 139.

support of PSC-CUNY, and support from AFOSR/NI (Instrumentation Grant F49620-00-1-0352).

Supporting Information Available: Tables giving IR frequencies and NMR isotropic chemical shifts for **I**−**IV** and crystallographic coordinates for **I**, **III**, and **IV** and a figure showing the calculated solid-state NMR spectra for a hypothetical $^{51}V(V)$-containing diamagnetic solid (CIF, PDF). This material is available free of charge via the Internet at http://pubs.acs.org.

JA029246P